

Chaotic Oscillations of Spacecraft with an Elastic Radially Oriented Tether

V. S. Aslanov and A. S. Ledkov

Samara State Aerospace University Moskovskoye sh. 34,
Samara 443086, Russia

e-mail: aslanov_vs@mail.ru, ledkov@inbox.ru

Received August 25, 2010

Abstract—A mechanical system consisting of a spacecraft with weightless elastic tether and load is considered in the paper. The spacecraft motion under the action of tensile force of a radially oriented tether is investigated. It is shown that elastic tether oscillations can result in appearance of chaotic modes of spacecraft motion. By means of the Melnikov method a condition is obtained, allowing one to determine the measure of damping sufficient for prevention of these chaotic modes. The influence of system's mass-geometric and elastic characteristics on the form of phase portrait and on the value of periodic disturbance, caused by oscillations of the elastic vertical tether, is studied.

DOI: 10.1134/S0010952512020013

1. PROBLEM FORMULATION

Space tether systems (STS) differ from conventional spacecraft in a great extension, variable configuration, and capability of interacting with the Earth's magnetic field [1]. Owing to these features the spectrum of tasks, where STS can be applied, is extremely wide. These tasks include both various transportation operations [2–5], and electric power generation [6, 7], and deep space exploration [8, 9]. Some of these projects can be implemented already now; others demand more advanced technologies [10]. The projects, which are planned to be realized in the nearest future, have some specific features. First, many of them suggest the use of radially oriented STS. For example, the STS intended for sounding the Earth surface will operate in such a regime [11]. Another task suggesting the use of radial links is the problem of lifting the load from a low-altitude orbit, when a docking interface is dropped from an orbital spacecraft on a tether, the system is oriented along the local vertical and remains in such a position up to connection with a load [12]. The second feature of mentioned projects is STS construction on the multi-purpose spacecraft basis, which imposes additional safety requirements, because STS operation should not hinder and threaten execution of other scheduled works and experiments.

Numerous research works are devoted to the problem of studying the STS dynamics. In the majority of them the main attention is given to modeling the tether, choosing the control law, and to studying stability issues. In so doing, the ultimate bodies connected by a tether are considered as material points [13, 14,

15]. Meanwhile, the tether can exert a significant effect on the motion relative to the center of mass of a carrying spacecraft [16], and the periodic character of elastic radial tether oscillations makes premises for origination of chaotic modes of motion which, ultimately, can lead to tether reeling on a spacecraft [17].

This work states the problem of studying chaotic modes of motion relative to the center of mass of a spacecraft, carrying a radial elastic tether, and searching for the techniques of avoiding chaotic modes on the basis of methods of chaotic dynamics [18].

2. MATHEMATICAL MODEL

We consider the mechanical system consisting of a spacecraft, weightless elastic tether, and a load (Fig. 1). The spacecraft represents a solid body with the center of mass at point D_1 , and the load is a material point D_2 . Spacecraft's and load's masses are m_1 and m_2 , respectively; A , B , and C are the principal moments of inertia of the spacecraft.

We suppose the spacecraft's center of mass to move over a circular orbit with constant angular velocity $\omega = \sqrt{\mu r^{-3}}$, where μ is the gravitational parameter, and r is the geocentric distance. In the process of motion the spacecraft is influenced only by the gravitational moment and by the moment of tether tension force. Let the tether be turned along the local vertical. The radial position of the system is stable [19]. We also assume the tether length to be considerably greater than the spacecraft size, $l \gg \Delta$, and considerably smaller than the radius of orbit, $l \ll r$.

The STS kinetic energy is composed of spacecraft kinetic energy T_1 and load kinetic energy T_2 .

$$T_1 = \frac{m_1 r^2 \omega^2}{2} + \frac{1}{2} C(\dot{\alpha} + \omega)^2, \quad T_2 = \frac{m_2 V_2^2}{2}, \quad (2.1)$$

where α is the angle between spacecraft's longitudinal axis and the local vertical, V_2 is the absolute velocity of the load

$$V_2^2 = \dot{x}_2^2 + \dot{y}_2^2,$$

x_2, y_2 are load coordinates in the inertial coordinate system OXY :

$$\begin{aligned} x_2 &= r \cos \vartheta - \Delta \cos(\alpha + \vartheta) - l \cos(\varphi + \vartheta), \\ y_2 &= r \sin \vartheta - \Delta \sin(\alpha + \vartheta) - l \sin(\varphi + \vartheta), \end{aligned}$$

where ϑ is the angle of true anomaly of the spacecraft's center of mass, and φ is the angle of tether deviation from the local vertical.

The potential energy of a system is equal to the sum of potential energy of the gravitational field W_G [20] and potential energy of an elastic tether W_E

$$\begin{aligned} W_G &= -\frac{\mu m_1}{r} - \frac{\mu m_2}{r_2} + \frac{3}{2} \frac{\mu}{r^3} (A - B) \cos^2 \alpha, \\ W_E &= \frac{c}{2} (l - l_0)^2, \end{aligned} \quad (2.2)$$

where $c = ES l_0^{-1}$ is the tether rigidity, E is the Young's modulus, S is the tether's cross-section area, l_0 is the undeformed tether length. Since the spacecraft's center of mass moves over a circular orbit, $\mu = \omega^2 r^3$ and

$$W_G = -\omega^2 r^2 m_1 - \frac{m_2 \omega^2 r^3}{r_2} + \frac{3}{2} \omega^2 (A - B) \cos^2 \alpha.$$

Let us consider the ratio r^3/r_2 appearing in the second term. Supposing l/r and Δ/r to be small quantities of order of ε , we expand it into a series having retained the terms of the order of ε^2 :

$$\begin{aligned} \frac{r^3}{r_2} &= \frac{r^3}{\sqrt{x_2^2 + y_2^2}} \approx \frac{r^2}{\sqrt{1 - 2\frac{l}{r} \cos \varphi + \frac{l^2}{r^2}}} \approx r^2 \\ &+ r l \cos \varphi + r \Delta \cos \alpha - (1 - 3 \cos^2 \varphi) \frac{l^2}{2} \\ &- (1 - 3 \cos^2 \alpha) \frac{\Delta^2}{2} + (2 \cos \alpha \cos \varphi - \sin \alpha \sin \varphi) \Delta l. \end{aligned}$$

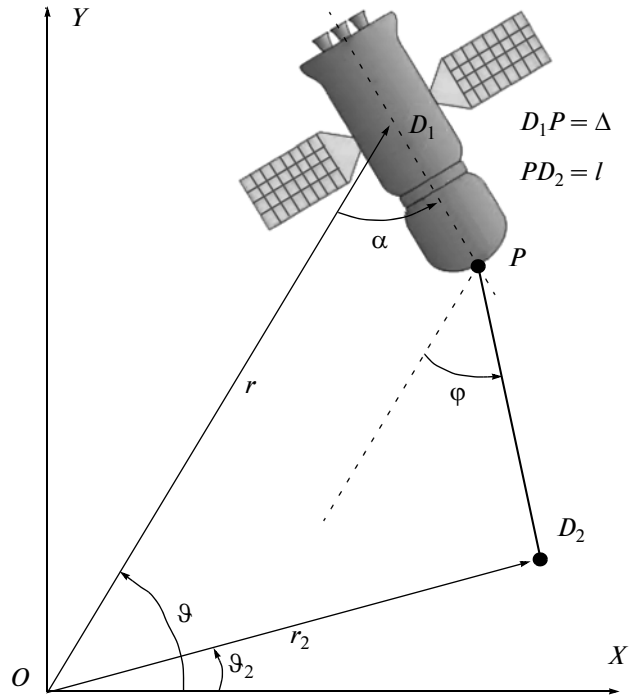


Fig. 1.

Then

$$\begin{aligned} W_G &= -\omega^2 r^2 m_1 - m_2 \omega^2 \\ &\times \left(r^2 + r l \cos \varphi + r \Delta \cos \alpha - (1 - 3 \cos^2 \varphi) \frac{l^2}{2} \right. \\ &\left. - (1 - 3 \cos^2 \alpha) \frac{\Delta^2}{2} + (2 \cos \alpha \cos \varphi - \sin \alpha \sin \varphi) \Delta l \right) \\ &+ \frac{3}{2} \omega^2 (A - B) \cos^2 \alpha. \end{aligned} \quad (2.3)$$

The Lagrangian of a system has the form

$$\begin{aligned} L &= \frac{3m_1 r^2 \omega^2}{2} + \frac{1}{2} C(\omega + \dot{\alpha})^2 \\ &- \frac{3}{2} \omega^2 (A - B) \cos^2 \alpha - \frac{c}{2} (l - l_0)^2 \\ &+ m_2 \Delta [l \cos(\alpha - \varphi) (\dot{\alpha} \omega + \dot{\varphi} \omega + \dot{\alpha} \dot{\varphi}) \\ &- \dot{l} (\dot{\alpha} + \omega) \sin(\alpha - \varphi)] - m_2 r \omega [\dot{l} \sin \varphi \\ &+ l \dot{\varphi} \cos \varphi + \Delta \dot{\alpha} \cos \alpha] + \frac{m_2}{2} [\dot{\varphi} l^2 (\dot{\varphi} + 2\omega) \\ &+ \Delta^2 \dot{\alpha} (\dot{\alpha} + 2\omega) + 3\omega^2 (r^2 + (l \cos \varphi + \Delta \cos \alpha)^2) + \dot{l}^2]. \end{aligned} \quad (2.4)$$

Now we write the Lagrange equations of the second kind using the tether length l and angles α and φ as generalized coordinates.

$$\frac{d}{dt} \frac{dL}{dq_i} - \frac{dL}{dq_i} = Q_{q_i}, \quad q_i = \alpha, l, \varphi, \quad (2.5)$$

where $Q_\alpha = Q_l = Q_\varphi = 0$. Having resolved the Lagrange equations for second derivatives, we get

$$\begin{aligned} \ddot{\alpha} &= \frac{3}{2}\omega^2 \frac{(A-B)}{C} \sin 2\alpha - \frac{\Delta c}{C} (l-l_0) \sin(\alpha-\varphi), \\ \ddot{l} &= -\frac{c(l-l_0)}{2C} \left(\Delta^2 + 2\frac{C}{m_2} - \Delta^2 \cos(2\alpha-2\varphi) \right) \\ &+ 3\omega^2 \cos\varphi (l \cos\varphi + \Delta \cos\alpha) + 2l\omega\dot{\varphi} + \dot{\alpha}\Delta(\dot{\alpha} + 2\omega) \\ &\times \cos(\alpha-\varphi) + \dot{\varphi}^2 l + \frac{3\Delta\omega^2 \sin 2\alpha \sin(\alpha-\varphi)}{2C}, \quad (2.6) \\ \ddot{\varphi} &= \frac{\Delta^2 c}{2lC} (l-l_0) \sin(2\alpha-2\varphi) + \frac{\dot{\alpha}\Delta(\dot{\alpha} + 2\omega) \sin(\alpha-\varphi)}{l} \\ &- \frac{3\omega^2 \sin\varphi (l \cos\varphi + \Delta \cos\alpha)}{l} \\ &- \frac{2\dot{l}(\omega + \dot{\varphi})}{l} - \frac{3\Delta\omega^2 (A-B) \sin 2\alpha}{2lC}. \end{aligned}$$

In the case of vertical tether $\varphi=0$, $\dot{\varphi} = 0$ and Eq. (2.6) take on the form:

$$\begin{aligned} \ddot{\alpha} &= \frac{3}{2}\omega^2 \frac{(A-B)}{C} \sin 2\alpha - \frac{\Delta c}{C} (l-l_0) \sin \alpha, \quad (2.7) \\ \ddot{l} &= -\frac{c(l-l_0)}{2C} \left(\Delta^2 + 2\frac{C}{m_2} - \Delta^2 \cos 2\alpha \right) \\ &+ 3\omega^2 (l + \Delta \cos \alpha) \quad (2.8) \\ &+ \dot{\alpha}\Delta(\dot{\alpha} + 2\omega) \cos \alpha + \frac{3\Delta\omega^2 \sin 2\alpha \sin \alpha}{2C}. \end{aligned}$$

Considering Δ as a small quantity, we write Eq. (2.8) in the form

$$\ddot{l} = -\frac{c}{m_2} (l-l_0) + 3\omega^2 l = -l \left(\frac{c}{m_2} - 3\omega^2 \right) + \frac{c}{m_2} l_0$$

or

$$\ddot{l} + \Omega^2 l = ES/m_2, \quad (2.9)$$

where $\Omega = \sqrt{\frac{c}{m_2} - 3\omega^2} = \sqrt{\frac{ES}{m_2 l_0} - 3\omega^2}$.

Equation (2.9) has the analytical solution

$$l = l_1 + \frac{V_0}{\Omega} \sin \Omega t, \quad (2.10)$$

where $l_1 = \frac{c l_0}{m_2 \Omega^2} = \frac{ES}{m_2 \Omega^2}$. Presented equations are valid in the case when the tether is at the extended state. This condition is fulfilled, if

$$V_0 < 3\omega^2 l_0 / \Omega. \quad (2.11)$$

Substituting solution (2.10) into (2.7), we get

$$\ddot{\alpha} = -a \sin \alpha - c \sin \alpha \cos \alpha - \varepsilon \sin \alpha \sin \Omega t, \quad (2.12)$$

where $a = \frac{\Delta 3\omega^2 ES}{C \Omega^2}$, $c = 3\omega^2 \frac{B-A}{C}$, $\varepsilon = \frac{\Delta V_0 ES}{C \Omega l_0}$. Condition (2.11) can be written as

$$\varepsilon < a. \quad (2.13)$$

The system's dynamics is determined by the ratio of coefficients a , c , and ε , which, in turn, depend on STS characteristics. The form of a phase portrait of an undisturbed system ($\varepsilon = 0$) depends on the parameter

$$\gamma = \frac{c}{a} = \frac{B-A}{\Delta} \left(\frac{1}{m_2 l_0} - \frac{3\omega^2}{ES} \right). \quad (2.14)$$

Numerical calculations have shown that, for example, for the STS, whose parameters are close to those used within the framework of the YES-2 experiment [21], coefficients c and ε have the same order of magnitude, and for some values of V_0 coefficient ε can exceed c . In this case it makes sense to use, instead of Eq. (2.12), the following equation

$$\ddot{\alpha} = -a \sin \alpha - \varepsilon (\sin \alpha \sin \Omega t + b \sin \alpha \cos \alpha), \quad (2.15)$$

where $b = \frac{3\omega^2 \Omega l_0 (B-A)}{\Delta V_0 ES}$. Equation (2.15) describes the disturbed motion of a mathematic pendulum.

3. BIFURCATION DIAGRAM

The existence of a periodic disturbance in Eqs. (2.12), (2.14) forms precondition for chaotization of the spacecraft motion. A chaotic layer arises in the environs of a separatrix of an undisturbed system. The phase trajectory falling into this layer can result in transition from an oscillatory mode of motion into rotational one, which is quite dangerous, because it can cause tether reeling on a spacecraft.

One of basic techniques of chaotic dynamics, which allows one to estimate the chaotic layer thickness, is the Melnikov method. To apply it, one should obtain analytical solutions to homoclinic and heteroclinic trajectories of an undisturbed system:

$$\ddot{\alpha} = -a \sin \alpha - c \sin \alpha \cos \alpha. \quad (3.1)$$

The form of a phase portrait of Eq. (3.1) depends on the parameter $\gamma = c/a$. Figure 2 presents the bifurcation diagram and phase portraits obtained for various values of γ . One can distinguish three zones on the diagram: $\gamma < -1$, $-1 \leq \gamma \leq 1$, $\gamma > 1$. The solid and dashed thick lines, shown on the diagram, correspond to singular points of center and saddle types on the phase portrait of undisturbed system (3.1). White circles mark the bifurcation points, at which a sharp reconstruction of motion takes place. Examples of phase portraits for each zone are given in Fig. 2.

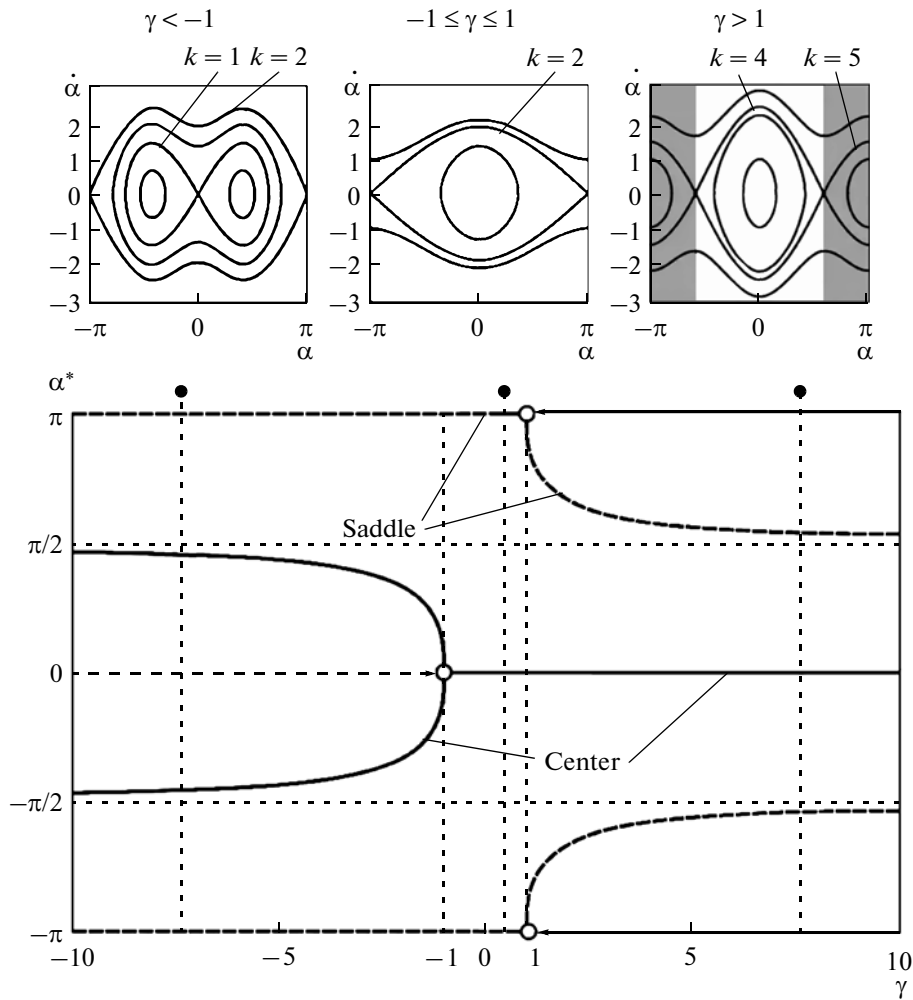


Fig. 2.

Saddle points, presented on phase portraits, are connected by separatrices. Equation (3.1) has the integral of energy

$$\frac{\dot{\alpha}^2}{2} + W(\alpha) = h,$$

where $W(\alpha) = -a\cos\alpha - c/2\cos^2\alpha$ is the potential energy, and h is the total energy. Substituting into this equation as h the energy, calculated at a saddle point α_s , and separating the variables, we obtain:

$$t = \int_{\alpha_0}^{\alpha} (2W(\alpha_s) - 2W(\alpha))^{-1/2} d\alpha.$$

Calculating this integral for various γ values, we obtain the equations describing the motion over separatrices (Table 1).

In the case $\gamma < -1$ two centers and three saddle points are observed on the phase portrait (Fig. 2). Sep-

aratrices divide the phase space into several zones: three oscillatory and two rotational ones. Several separatrix-type trajectories can be distinguished in the figure: heteroclinic, connecting saddle points $\alpha_s = -\pi, \alpha_s = \pi$ ($k = 2$, see Table 1) and homoclinic, connecting the saddle point $\alpha_s = 0$ with itself ($k = 1$, see Table 1). In the case $-1 \leq \gamma \leq 1$, two saddle points are observed on the phase portrait ($\alpha_s = -\pi, \alpha_s = \pi$), which are connected by a heteroclinic trajectory ($k = 2$, see Table 1) and one center $\alpha_s = 0$. At $\gamma > 1$ one observes three centers ($\alpha_c = -\pi, \alpha_c = 0, \alpha_c = \pi$), and two saddles connected by heteroclinic trajectories ($k = 4, k = 5$, see Table).

According to (2.14), γ is a function of the system's parameters. Let us investigate the influence of these parameters. Consider the second multiplier in (2.14):

$$\frac{1}{ml_0} - \frac{3\omega^2}{ES} \approx \frac{1}{ml_0} - \frac{\omega^2}{ER^2}, \tag{3.2}$$

Homo- and hetero-clinic trajectories

k	$\gamma = \frac{c}{a}$	Equations for a trajectory
1	$\gamma < -1$	$\alpha_{\pm}(t) = \pm 2 \arctan\left(\frac{d}{\cosh \lambda t}\right), \sigma_{\pm}(t) = (\dot{\alpha})_{\pm} = \mp \frac{2\lambda d \sinh \lambda t}{(\cosh \lambda t)^2 + d^2}, \lambda = \sqrt{-a-c}, d = \sqrt{-\frac{a+c}{a}}$
2	$\begin{matrix} \gamma \leq -1 \\ \gamma \leq 1 \end{matrix}$	$\alpha_{\pm}(t) = \pm 2 \arctan(d \sinh \lambda t), \sigma_{\pm}(t) = (\dot{\alpha})_{\pm} = \mp \frac{2\lambda d \cosh \lambda t}{1 + d^2 \sinh^2 \lambda t}, \lambda = \sqrt{a-c}, d = \sqrt{\frac{a}{a-c}}$
3	$\gamma = 0$	$\alpha_{\pm}(t) = \pm 2 \arctan(\sinh \sqrt{a} t), \sigma_{\pm}(t) = (\dot{\alpha})_{\pm} = \pm \frac{2\lambda \cosh \lambda t}{1 + \sinh^2 \lambda t}, \lambda = \sqrt{a}$
4	$\gamma > 1$	$\alpha_{\pm}(t) = \pm 2 \arctan\left(\tan \frac{\alpha_S}{2} \tanh \frac{\lambda t}{2}\right), \sigma_{\pm}(t) = (\dot{\alpha})_{\pm} = \pm \frac{\lambda \sin \alpha_S}{\cosh \lambda t + \cos \alpha_S}, \alpha_S = \pm \arccos\left(-\frac{1}{\gamma}\right), \lambda = \sqrt{\frac{c^2 - a^2}{c}},$ $d = -\frac{a}{c}$
5	$\gamma > 1$	$\alpha_{\pm}(t) = \pi \pm 2 \arctan\left(\cot \frac{\alpha_S}{2} \tanh \frac{\lambda t}{2}\right), \sigma_{\pm}(t) = (\dot{\alpha})_{\pm} = \frac{\lambda \sin \alpha_S}{\cosh \lambda t - \cos \alpha_S}, \alpha_S = \pm \arccos\left(-\frac{1}{\gamma}\right), \lambda = \sqrt{\frac{c^2 - a^2}{c}},$ $d = -\frac{a}{c}$

where R is the radius of cross-section of a tether. Having in mind performed experiments and those planned for the nearest future [1, 10, 12], let us estimate (3.2). For this purpose we determine the minimally possible order of a minuend and the maximally possible order of a subtrahend. For currently existing STS projects the tether can be a few tens of kilometers long, and the mass of a load does not exceed one ton; therefore, the minimal possible value of a minuend for existing programs is of the order of $10^{-8} \text{ kg}^{-1} \text{ m}^{-1}$. Near the Earth surface the angular velocity is $\omega = 1.242 \times 10^{-3} \text{ s}^{-1}$, and it decreases with increasing altitude of orbit. For the modern materials, used for manufacturing space tethers, the Young's modulus has the order of 10^{11} N/m^2 . The tether cross-section radius can constitute a value of the order of 10^{-4} m . Substituting these values into (3.2),

we find that the maximum order of a subtrahend is $10^{-9} \text{ kg}^{-1} \text{ m}^{-1}$. Even such a rough estimation allows one to conclude that for existing STS programs (and for those planned for the nearest future) quantity (3.2) is positive. In reality the difference between a subtrahend and minuend will be even greater, because the load mass and the tether length influence both the cross-section of a tether and the material of which it is manufactured. The above analysis allows us to conclude that the sign of γ is determined by the ratio of spacecraft's moments of inertia (Fig. 3). For $A < B$ the coefficient γ is greater than zero, and for $A > B$ it is smaller.

According to (2.14), the absolute value of γ decreases with increasing tether mass and load length, and it grows with increasing Δ , modulus of elasticity, and tether thickness. A change of the system's parameters influences not only the form of a phase portrait of an undisturbed system, but also the disturbing effect value. At $|\gamma| < 1$ the greatest contribution to system's dynamics is made by coefficient a , and at $|\gamma| > 1$ coefficient c produces biggest effect. Let us compare them with ε

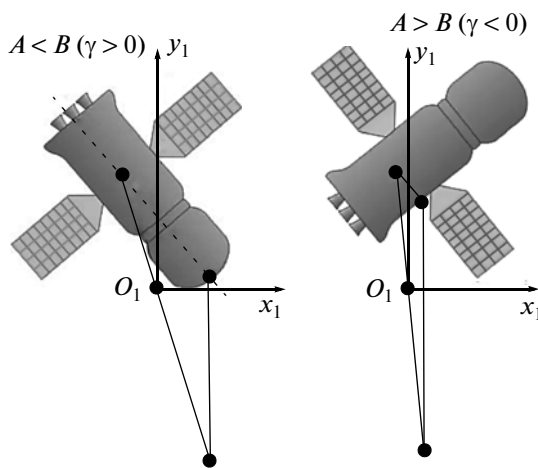


Fig. 3.

$$\eta_1 = \frac{\varepsilon}{a} = \frac{V_0 \sqrt{\frac{ES}{m_2 l_0} - 3\omega^2}}{3\omega^2 l_0}, \tag{3.3}$$

$$\eta_2 = \frac{\varepsilon}{c} = \frac{\Delta V_0 ES}{3\omega^2 (B - A) l_0 \sqrt{\frac{ES}{m_2 l_0} - 3\omega^2}}.$$

The smaller the parameters $\eta_j, (j = 1, 2)$, the weaker the influence exerted by a disturbance on a system. The analysis of (3.3) indicates that an increase of $E, S,$

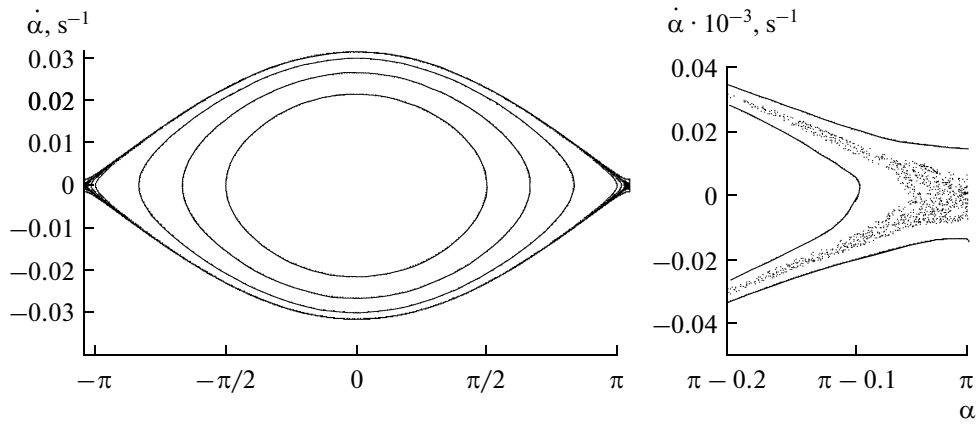


Fig. 4.

and V_0 results in increasing η_1 and η_2 ; an increase of m_2 results in decreasing η_1 and increasing η_2 ; an increase of l_0 results in decreasing η_1, η_2 ; and an increase of Δ results in increasing η_2 without influencing η_1 .

4. CHAOTIC MOTION

We construct Poincaré’s cross sections for Eq. (2.12). Let the STS have the following parameters: $m_2 = 20$ kg, $A = 3000$ kg m², $B = C = 10^4$ kg m², $\Delta = 1$ m, $l_0 = 30$ km, $ES = 5$ kN, $V_0 = 0.01$ m/s, and $\omega = 1.172 \times 10^{-3}$ s⁻¹. In this case, coefficients of Eq. (2.12) are equal to

$$a = 2.473 \cdot 10^{-4}, c = 2.884 \cdot 10^{-6}, \varepsilon = 1.826 \cdot 10^{-6}.$$

Figure 4 shows the Poincaré’s cross section. The chaotic layer is seen in the environs of a separatrix of an undisturbed system. One should note that the thickness of this layer is rather small.

A more interesting picture is observed in the case of strong disturbances. Figure 5 shows the Poincaré’s cross section for a system which differs from that considered only in the initial velocity $V_0 = 1$ m/s. In this case $a = 2.473 \times 10^{-4}$, $c = 2.884 \times 10^{-6}$, $\varepsilon = 1.826 \times 10^{-4}$. Figure 6 shows the motion of a system with $a = 2.479 \times 10^{-3}$, $c = 2.884 \times 10^{-6}$, $\varepsilon = 8.175 \times 10^{-4}$ ($m_2 = 100$ kg, $V_0 = 1$ m/c, $\Delta = 2$ m). It is seen that a rather wide chaotic layer exists in the environs of a separatrix of an undisturbed system. One can also notice the existence of new zones of stable oscillations (A1 and A2 in Fig. 6).

5. MELNIKOV METHOD

As it was noted above, the presence of chaos in a system can result in some undesirable effects. Inclusion of various dissipation components into a system can serve as a technique of eliminating chaotic modes.

For example, in paper [22] it was proposed to use a spherical hinge. In this case one should take into account in Eqs. (2.5) the force of viscous friction

$$Q_\alpha = \delta C \dot{\alpha},$$

which will result in appearance of the additional term $-\delta \dot{\alpha}$ in the right-hand side of Eq. (2.12)

$$\ddot{\alpha} = -a \sin \alpha - c \sin \alpha \cos \alpha - \varepsilon \sin \alpha \sin \Omega t - \delta \dot{\alpha}. \quad (5.1)$$

Here, δ is the damping coefficient. On the basis of Melnikov method [6] we determine quantity δ sufficient for eliminating chaotic modes.

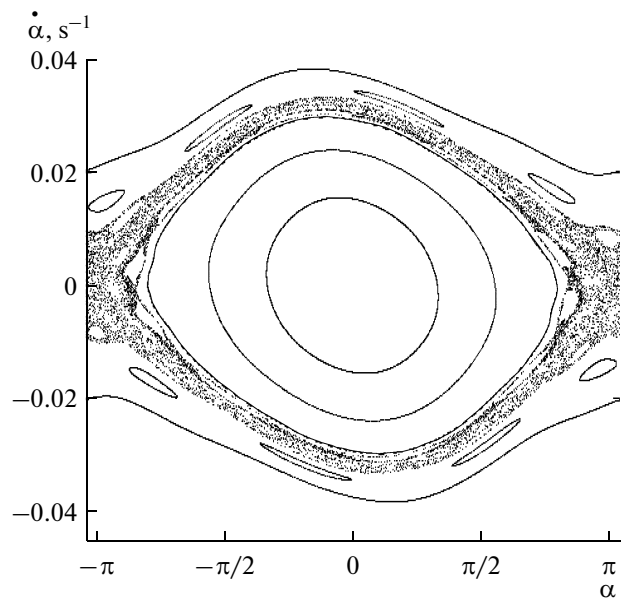


Fig. 5.

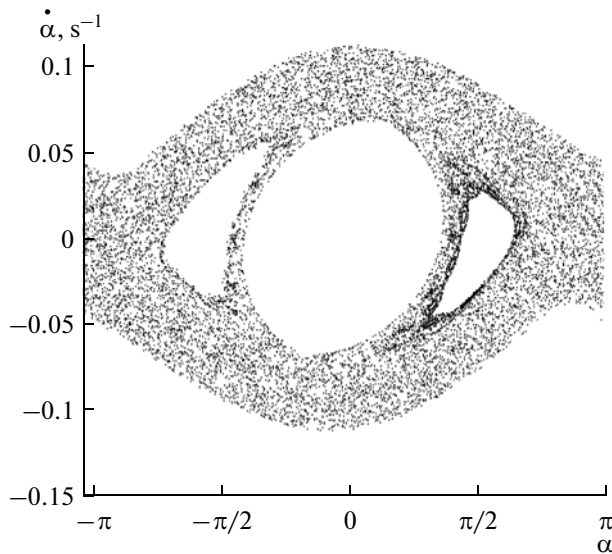


Fig. 6.

Now we rewrite (5.1) in the form suitable for the use of Melnikov method

$$\begin{aligned} \dot{\alpha} &= \sigma = f_1 + g_1, \\ \dot{\sigma} &= f_2 + g_2, \end{aligned} \tag{5.2}$$

where $f_1 = \sigma$, $g_1 = 0$, $f_2 = -a \sin \alpha - c \sin \alpha \cos \alpha$, $g_2 = -\varepsilon \sin \alpha \sin \Omega t - \delta \sigma$. For disturbed system (5.2) we write the Melnikov's function:

$$M^\pm(t_0) = \int_{-\infty}^{\infty} (f_1 g_2 - f_2 g_1) dt = M_\varepsilon + M_\delta, \tag{5.3}$$

where

$$M_\varepsilon = -\varepsilon \int_{-\infty}^{\infty} \sigma_\pm \sin \alpha_\pm \sin \Omega(t + t_0) dt, \tag{5.4}$$

$$M_\delta = -\delta \int_{-\infty}^{\infty} \sigma_\pm^2 dt. \tag{5.5}$$

According to the Melnikov method, the condition of chaos existence in the system can be written as

$$M_\delta < M_\varepsilon. \tag{5.6}$$

Let us present functions (5.4) and (5.5) in the forms

$$M_\varepsilon^{(k)} = -\varepsilon \int_{-\infty}^{\infty} \sigma_\pm^{(k)} \sin \alpha_\pm^{(k)} \sin \Omega(t + t_0) dt, \tag{5.7}$$

$$M_\delta^{(k)} = -\delta \int_{-\infty}^{\infty} (\sigma_\pm^{(k)})^2 dt = \delta J_\pm^{(k)}, \tag{5.8}$$

where index k determines expressions for a homo/hetero-clinical trajectory (see Table).

Now we simplify integral (5.7)

$$\begin{aligned} & \int_{-\infty}^{\infty} \sigma_\pm^{(k)} \sin \alpha_\pm^{(k)} \sin \Omega(t + t_0) dt \\ &= \int_{-\infty}^{\infty} \sigma_\pm^{(k)} \sin \alpha_\pm^{(k)} (\sin(\Omega t) \cos(\Omega t_0) \\ & \quad + \cos(\Omega t) \sin(\Omega t_0)) dt \\ &= \int_{-\infty}^{\infty} \sigma_\pm^{(k)} \sin \alpha_\pm^{(k)} \sin(\Omega t) \cos(\Omega t_0) dt \\ & \quad + \int_{-\infty}^{\infty} \sigma_\pm^{(k)} \sin \alpha_\pm^{(k)} \cos(\Omega t) \sin(\Omega t_0) dt. \end{aligned}$$

The integrand of the first term, in virtue of solutions given in Table, is an odd function of variable t ; therefore, the first term is equal to zero, and (5.7) can be written in the form

$$\begin{aligned} & \int_{-\infty}^{\infty} \sigma_\pm^{(k)} \sin \alpha_\pm^{(k)} \sin \Omega(t + t_0) dt \\ &= \sin(\Omega t_0) \int_{-\infty}^{\infty} \sigma_\pm^{(k)} \sin \alpha_\pm^{(k)} \cos(\Omega t) dt = \sin(\Omega t_0) I_\pm^{(k)}, \end{aligned}$$

then

$$M_\varepsilon^{(k)} = -\varepsilon I_\pm^{(k)} \sin(\Omega t_0).$$

The improper integrals

$$I_\pm^{(k)} = \int_{-\infty}^{\infty} \sigma_\pm^{(k)} \sin \alpha_\pm^{(k)} \sin(\Omega t) dt, \quad J_\pm^{(k)} = \int_{-\infty}^{\infty} (\sigma_\pm^{(k)})^2 dt \tag{5.9}$$

are calculated with accounting for solutions given in Table:

$$I_\pm^{(1)} = \pm 2d^2 \int_{-\infty}^{\infty} \frac{\text{sh } 2\tau}{(\text{ch}^2 \tau + d^2)^2} \sin \bar{\Omega}_1 \tau d\tau,$$

$$J_\pm^{(1)} = \pm 4d^2 \lambda \int_{-\infty}^{\infty} \left[\frac{\text{sh } \tau}{\text{ch}^2 \tau + d^2} \right]^2 d\tau,$$

$$I_\pm^{(2)} = \pm d^2 \int_{-\infty}^{\infty} \frac{\text{sh } 2\tau}{(d^2 \text{sh}^2 \tau + 1)^2} \sin \bar{\Omega}_2 \tau d\tau,$$

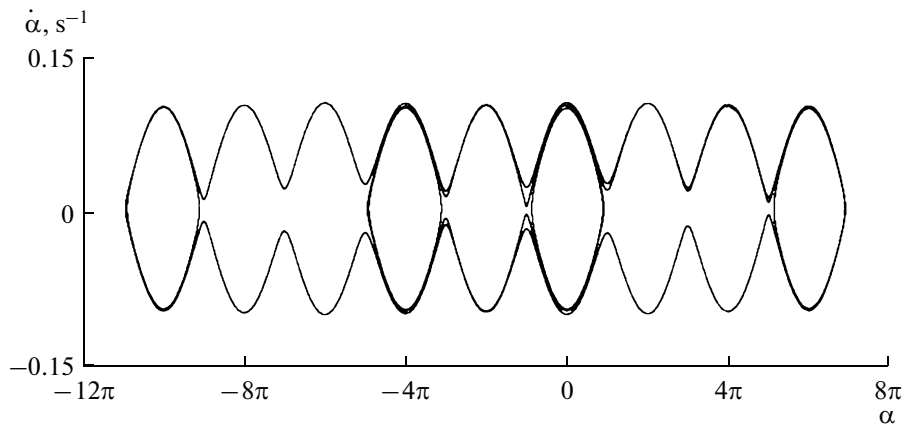


Fig. 7.

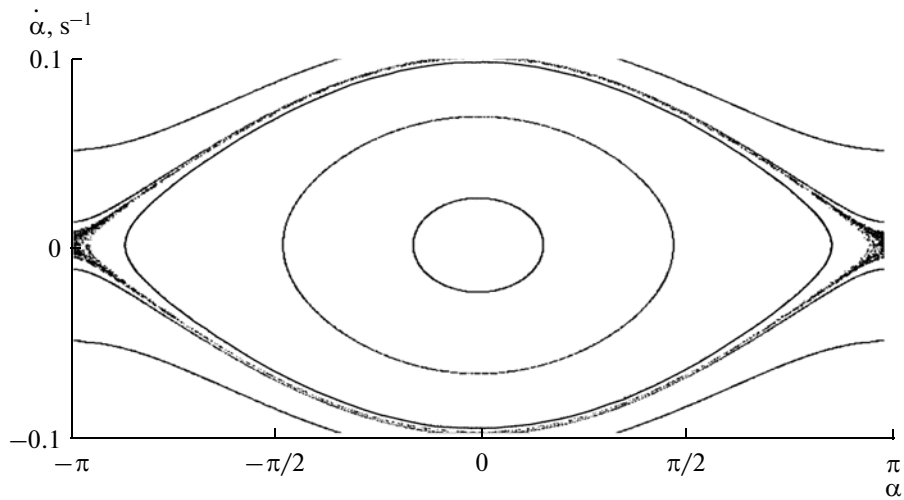


Fig. 8.

$$\begin{aligned}
 J_{\pm}^{(2)} &= \pm 4d^2\lambda \int_{-\infty}^{\infty} \left[\frac{\text{ch } \tau}{1 + d^2 \text{sh}^2 \tau} \right]^2 d\tau, & J_{\pm}^{(4)} &= \pm \lambda \int_{-\infty}^{\infty} \left[\frac{\sin \alpha_S}{\text{ch } \tau + \cos \alpha_S} \right]^2 d\tau, \\
 I_{\pm}^{(3)} &= \pm \int_{-\infty}^{\infty} \frac{\text{sh } 2\tau}{(\text{sh}^2 \tau + 1)^2} \sin \bar{\Omega}_2 \tau d\tau, & I_{\pm}^{(5)} &= \pm (1 - d^2) \int_{-\infty}^{\infty} \frac{\text{sh } \tau}{(\text{ch } \tau - d)^2} \sin \bar{\Omega}_5 \tau d\tau, \\
 J_{\pm}^{(3)} &= \pm 4\lambda \int_{-\infty}^{\infty} \left[\frac{\text{ch } \tau}{1 + \text{sh}^2 \tau} \right]^2 d\tau, & J_{\pm}^{(5)} &= \pm \lambda \int_{-\infty}^{\infty} \left[\frac{\sin \alpha_S}{\text{ch } \tau - \cos \alpha_S} \right]^2 d\tau, \\
 I_{\pm}^{(4)} &= \pm (1 - d^2) \int_{-\infty}^{\infty} \frac{\text{sh } \tau}{(\text{ch } \tau + d)^2} \sin \bar{\Omega}_4 \tau d\tau, & \bar{\Omega}_i &= \Omega/\lambda, \quad \tau = \lambda t,
 \end{aligned}$$

where λ and d are the coefficients given in Table.

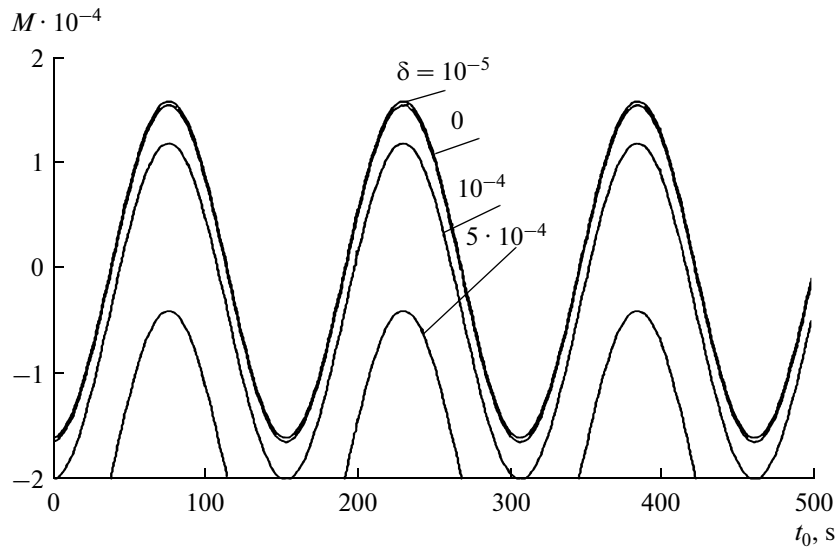


Fig. 9.

Let us introduce a new parameter $\Delta_0 = \delta/\varepsilon$; then the chaos existence condition in system (5.6) can be written as

$$\Delta_0 < \Delta_k = I_{\pm}^{(k)} / J_{\pm}^{(k)}. \quad (5.10)$$

By virtue of solutions presented in Table and integrals $I_{\pm}^{(k)}$ and $J_{\pm}^{(k)}$, Δ_k depend on the STS parameters.

$$\Delta_k = \Delta_k(A, B, C, \Delta, m, l_0, E, S, V_0). \quad (5.11)$$

With the purpose of verifying condition (5.10) we investigate the behavior of a disturbed system in the separatrix environs. Let $m_1 = 6000$ kg, $m = 100$ kg, $A = 2500$ kg m², $B = C = 10^4$ kg m², $\Delta = 2$ m, $l_0 = 30$ km,

$ES = 5000$ N, and $V_0 = 0.01$ m/s. The spacecraft moves over a circular orbit at the altitude $H = 250$ km ($p = 6621$ km), its angular velocity equals $\omega = 1.172 \cdot 10^{-3}$ s⁻¹. In this case the coefficients in the system (4.10) are equal to: $a = 2.482 \cdot 10^{-3}$, $c = 3.131 \cdot 10^{-5}$, $\varepsilon = 6.338 \cdot 10^{-5}$, $\Omega = 4.077 \cdot 10^{-2}$, $\gamma = 1.261 \cdot 10^{-3}$, and the case corresponding to $k=2$ is realized (see Table). Consider now the behavior of a system in the presence of a dissipative component in it. Let $\delta = 5 \cdot 10^{-6}$, then

$$\Delta_0 = 7.889 \cdot 10^{-2}, \quad \Delta_4 = 6.341.$$

In this case condition (5.10) is fulfilled, and the Melnikov's function has simple zeros. Therefore, chaos is present in the system, and phase trajectories can intersect the separatrix going over from the region of oscillation motions into the region of rotation and vice versa (Figure 7). Figure 8 shows the Poincaré's cross-section of a disturbed system.

As damping coefficient δ increases, the plot of the Melnikov's function is displaced downwards (Fig. 9); in this case the difference between Δ_0 and Δ_i decreases. It is seen from Fig. 10 that at some value of $\delta = \delta_*$ the plots of functions Δ_0 and Δ_i are intersected. In this case, condition (5.10) ceases to be fulfilled, and no chaos is observed in the system.

It is seen from Fig. 10, that quantity δ_* has the order of 10^{-4} , which exceeds the order of c and ε coefficients of system (2.12). In this case for applying the approach described above it is necessary to use Eq. (2.15). In this case the coefficients of system (5.2)

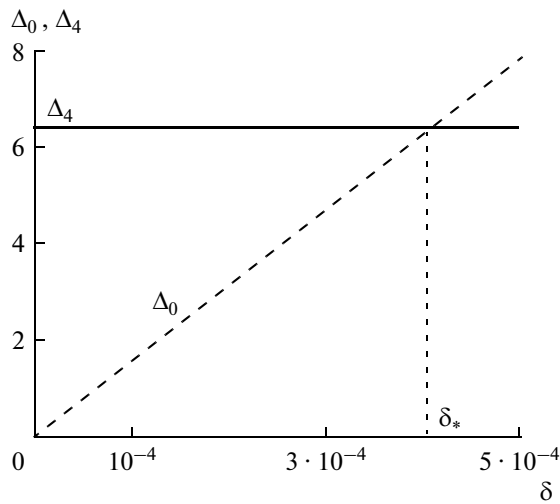


Fig. 10.

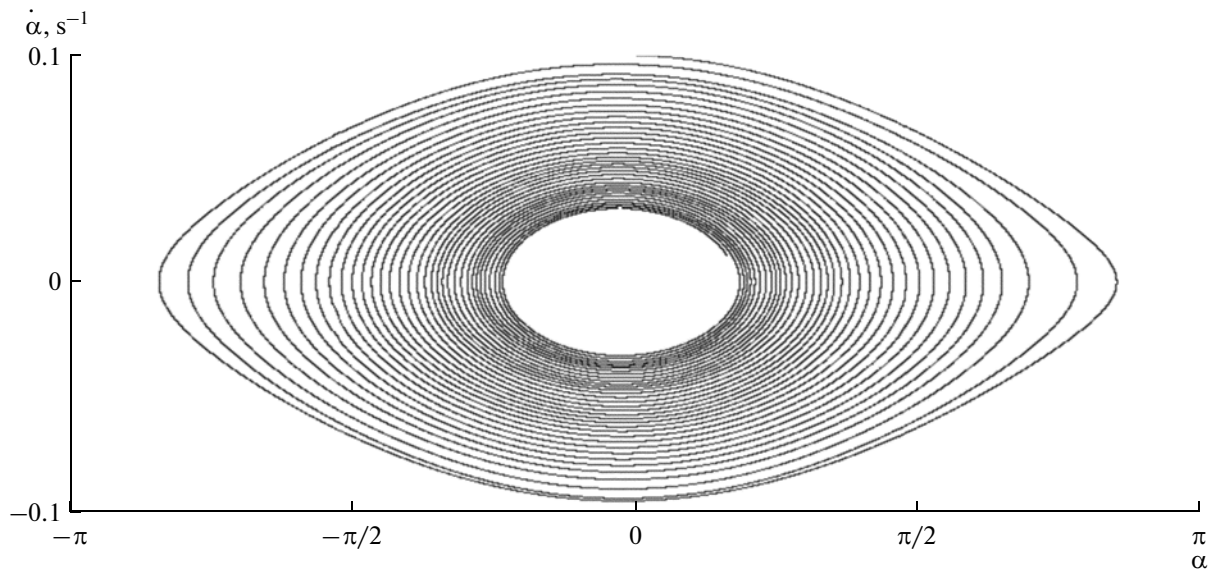


Fig. 11.

become: $f_1 = \sigma, g_1 = 0, f_2 = -a \sin \alpha, g_2 = -\varepsilon(\sin \alpha \sin \Omega t + b \sin \alpha \cos \alpha) - \delta \sigma$, and expression (5.4) is found as

$$M_\varepsilon = -\varepsilon \int_{-\infty}^{\infty} \sigma_{\pm} \left[\sin \alpha_{\pm} \sin \Omega(t + t_0) + \frac{c}{\varepsilon} \sin \alpha_{\pm} \cos \alpha_{\pm} \right] dt = -\varepsilon \int_{-\infty}^{\infty} \sigma_{\pm} \sin \alpha_{\pm} \sin \Omega(t + t_0) dt - c \int_{-\infty}^{\infty} \sigma_{\pm} \sin \alpha_{\pm} \cos \alpha_{\pm} dt - \varepsilon \int_{-\infty}^{\infty} \sigma_{\pm} \sin \alpha_{\pm} \sin \Omega(t + t_0) dt.$$

Here, $\alpha_{\pm}(t)$ and $\sigma_{\pm}(t)$ correspond to the case demonstrated in Table. Addition of a new term into g_2 does not influence the Melnikov's function in any way, and condition (5.10) conserves its form.

Consider the spacecraft motion for $\delta = 5 \cdot 10^{-4}$. In this case $\delta > \delta_*$, $\Delta_0 = 7.889$, $\Delta_4 = 6.341$ and condition (5.10) is not fulfilled, the Melnikov's function has no simple zeros (Fig. 9) and there is no chaos in the system. Figure 11 shows one phase trajectory for the initial conditions given above. It is seen that the trajectory does not intersect the separatrix of an undisturbed system, smoothly approaching the center $\alpha_* = 0$.

ACKNOWLEDGMENTS

This work was supported by the Russian Foundation for Basic Research, project no. 09-01-00384.

REFERENCES

1. Beletskii, V.V. and Levin, E.M., *Dinamika kosmicheskikh trosovykh sistem* (Dynamics of Space Tethered Systems), Moscow: Nauka, 1990.
2. Zimmermann, F., Schottle, U.M., and Messerschmid, E., Optimization of the Tether-Assisted Return Mission of a Guided Re-Entry Capsule, *Aerospace Science and Technology*, 2005, no. 9, pp. 713–721.
3. Beletskii, V.V., Ivanov, M.B., and Otstavnov, E.I., Model Problem of a Space Elevator, *Kosm. Issled.*, 2005, vol. 43, no. 2, pp. 157–160. [*Cosmic Research*, p. 152].
4. Williams, P., Blanksby, C., Trivailoa, P., and Fujii, H.A., In-Plane Payload Capture Using Tethers, *Acta Astronaut.*, 2005, vol. 57, pp. 772–787.
5. Ziegler, S.W. and Cartmell, M.P., Using Motorized Tethers for Payload Orbital Transfer, *J. Spacecr. Rockets*, 2001, vol. 38, no. 6, pp. 904–913.
6. McCoy, J.E., Electrodynamic Tethers, *Proc. 35th Intern. Astronautical Congress, Lausanne, Switzerland, October 7–13, 1984*, pp. 84–440.
7. Sorensen, K., Momentum Exchange Electrodynamic Reboost Tether. Technology Assessment Group Final Report, *Space Propulsion Technologies Program, July 24, 2003*, NASA Marshall Space Flight Center, Huntsville, AL 35812, 2003.
8. Bombardelli, C., Lorenzini, E.C., and Quadrelli, M.B., Retargetting Dynamics of a Linear Tethered Interferometer, *J. Guidance Control Dynam.*, 2004, vol. 27, no. 6, pp. 1061–1067.
9. Nordley, G., Tether-Tossed Mars Mission Examples, *Proceed. of the 37th AIAA/ASME/SAE/ASEE Joint Propulsion Conference and Exhibit [AIAA 2001-3375]*, 2001.

10. Eiden, M. and Cartmell, M.P., Overcoming the Challenges: Tether Systems Roadmap for Space Transportation Applications, *Proceed. of the AIAA/ICAS Intern. Air and Space Symposium and Exposition, Dayton, 14–17 July, 2003* [AIAA 2003-2840].
11. Ivanov, V.A., Tethered Systems in Space, *Aviats. Kosmonavtika*, 1984, no. 5, pp. 43–44.
12. Cartmell, M.P. and McKenzie, D.J., A Review of Space Tether Research, *Progress in Aerospace Sciences*, 2008, vol. 44, pp. 1–21.
13. Aslanov, V.S., Ledkov, A.S., and Stratilatov, N.R., Spatial Motion of a Space Tethered System Designed to Deliver Payload to the Earth, *Polyot*, 2007, no. 2, pp. 28–33.
14. Sazonov, V.V., Mathematical Modeling of Deployment of a Tethered System Taking the Tether Mass into Account, *Preprint of Keldysh Inst. of Applied Math., Russ. Acad. Sci.*, Moscow, 2006.
15. Dignat, F. and Shilen, V., Control of Vibrations of an Orbital Tethered System, *Prikl. Mat. Mekh.*, 2000, vol. 64, no. 5, pp. 747–754.
16. Aslanov, V.S., Ledkov, A.S., and Stratilatov, N.R., Influence of Tethered System of a Cargo Spacecraft on Its Attitude Motion, *Polyot*, 2009, no. 1, pp. 54–60.
17. Pirozhenko, A.V., Chaotic Regimes of Motion in Dynamics of Space Tethered Systems: 2. Mechanical Aspect of Phenomena, *Kosmichna Nauka i Tekhnol.*, 2001, vol. 7, no. 2/3, pp. 90–99.
18. Mel'nikov, V.K., Stability of the Center at Time-Periodic Disturbances, *Trudy Moskovskogo Matematicheskogo Obshchestva*, 1963, vol. 12, pp. 1–57.
19. Sadv, Yu.A., Forms of Equilibria of a Flexible Tether in the Plane of a Circular Orbit: 0- and 1-Parametric Families, Preprint of Keldysh Inst. of Applied Math., *Russ. Acad. Sci.*, Moscow, 2001, no. 68.
20. Beletskii, V.V., *Dvizhenie iskusstvennogo sputnika otositel'no tsentra mass* (Artificial Satellite Motion Relative to Its Center of Mass), Moscow: Nauka, 1965.
21. Williams, P., Hyslop, A., Stelzer, M., and Kruijff, M., Yes-2 Optimal Trajectories in Presence of Eccentricity and Aerodynamic Drag, *Acta Astronaut.*, 2009, no. 64, pp. 745–769.
22. Pirozhenko, A.V. and Khramov, D.A., A Scheme of Gravitational Stabilization of a Space Tethered System with a Spherical Hinge, *Tekhnicheskaya Mekhanika*, 2001, no. 1, pp. 136–148.